ELSEVIER

Revisiting the hydrogenation of sunflower oil over a Ni catalyst

María B. Fernández, Gabriela M. Tonetto, Guillermo H. Crapiste, Daniel E. Damiani *

PLAPIQUI (UNS-CONICET), Camino La Carrindanga Km 7, CC 717, CP 8000, Bahía Blanca, Argentina

Abstract

In the present paper the performance of commercial Ni catalyst in edible oil hydrogenation is evaluated under different operating conditions. Particularly, the influence of mass transport resistance on the *trans*-isomers selectivity is analyzed. Initially a series of experiments aim to analyze the effect of four process variables (reaction temperature, hydrogen bubbling device, agitation rate and stirrer design) on catalyst activity and selectivity to *trans*-isomers. These experiments are conducted in diffusional regimes. A simpler set of experiments is carried out operating under conditions that allow the authors to neglect some diffusional resistances although those associated to the catalyst are still present. In the first case activity and selectivity appear to be independent of the hydrogen bubbling system and the catalyst loading. The whole set of data analyzed in terms of the $C18:1/C18:2_0$ ratio as a function of the $C18:2/C18:2_0$ ratio shows that the former, a sort of selectivity, depends on the agitation regime. The formation of *trans*-isomers however, appears to be a function of the reaction extent only.

© 2007 Elsevier Ltd. All rights reserved.

Keywords: Hydrogenation; Nickel; Sunflower oil; *trans*-Isomers; SFC

1. Introduction

The hydrogenation of oils and fats and their derivates continues being one of the most versatile ways to modify the oxidative and thermal stability, the melting characteristics of the fat and its color. The hydrogenation can also alter physical properties of the raw material like the melting point, miscibility, surface tension, viscosity, etc.

The process is widely used in the elaboration of margarines, shortenings and products of bakery, as well as in the production of oleochemicals like fatty acids, alcohol and amines. The gradual elimination of the insaturations produces a progressive increase in the average melting point of the oil. Thus, the control over melting property can be attained through the specific knowledge on the partial hydrogenation process.

Most of natural oils present C–C double bonds in *cis* position. During the hydrogenation, along with the saturation of the double bonds, reactions of isomerization (geometric and positional) take place.

An increase in the *trans*-isomer content in the oil or the fat also produces an increase of its melting point. This has some advantages, as it is possible to reach higher melting points with small amounts of saturated fat, which is in principle attractive. Nevertheless, a series of medical papers that appeared in the first part of last decade alerted that the *trans*-isomers could have the same detrimental effect for health that the saturated fats. Mensink and Katan (1990) suggested that a diet rich in elaidic acid, compared to one rich in oleic acid, increases the total and low-density lipoprotein (LDL) cholesterol concentrations and decreases high-density lipoprotein (HDL) cholesterol concentration, hence resulting in a less favorable total-cholesterol:HDL-cholesterol ratio. Ascherio, Katan, Zock, Stampfer, and Willett (1999) demonstrated a dose-dependent relationship between *trans* fatty acid intake and the LDL:HDL ratio, and when combining a number of studies, the magnitude

---

* Corresponding author. Tel.: +54 0291 4861700; fax: +54 0291 4861600.

E-mail address: ddamiani@plapiqui.edu.ar (D.E. Damiani).

Nomenclature

Abbreviations

B	constant
C16.0	palmitic acid
C18.1c	oleic acid
C18.1t	elaidic acid
C18:0	stearic acid
C18:1	oleic acid
C18:2	linoleic acid
C18:3	linolenic acid
C20.0	arachidic acid
C22.0	behenic acid
C_i	concentration of component i (kmol/m^3)
C_{iS}	concentration of component i at exterior cata-lyst surface (kmol/m^3)
d	mean particle diameter (m)
D_{eff}	effective diffusion coefficient (m^2/s m$^3_{liq}$/m$^3_{cat}$)
$d_{stirrer}$	stirrer diameter (m)
Fr	Froude number, $Fr = N^2 d^2_{stirrer}/gH$
g	gravitational acceleration
Ga	Galileo number, $Ga = Re^2/Fr$
h_l	vortex depth
H	liquid height above impeller (m)
H$_2$	hydrogen
k	reaction constant
k_1a	volumetric gas–liquid mass transfer coefficient (s^{-1})
k_s	liquid to solid mass transfer coefficient (m s^{-1})
m	mass of catalyst
N	rotation rate (rev/s)
R	particle radius (m)
Re	Reynolds number, $Re = Nd^2_{stirrer}\rho/\mu$
r_{obs}	observed rate (mol/s kg$_{cat}$)
SFC	solid fat content

Greek letters

α, β	constants
Φ	Weisz–Prater criterion
η	effectiveness factor
μ	viscosity (Pa s)
ρ	density (kg m^{-3})
ϕ	Thiele modulus

Sub- and superscripts

i	component
p	particle

of this effect is greater for *trans* fatty acids compared to saturated fatty acids. There is nowadays a firm tendency in the industry towards lower levels of *trans*-isomers in fat.

The catalytic hydrogenation of vegetal oils has been widely studied (Patterson, 1994) and different models have been proposed to represent its kinetic (Mondal & Lalvani, 2000; Rodrigo, Daza, & Mendioroz, 1992). However, some recent reviews (Dijkstra, 1997) indicate that the kinetic and mechanisms of the hydrogenation process, especially those related to geometric and positional isomerization in triglycerides, are not completely known. On the other hand, studies of sunflower oil hydrogenation are relatively few (Rodrigo et al., 1992).

The hydrogenation is typically carried out in a three-phase semi batch reactor: hydrogen gas is bubbled in hot liquid oil (120–188 °C), usually under pressure (100–608 kPa). The reaction requires the use of a catalyst. Although it has been experienced with several metals, including the noble metals, the most widely used catalyst is powdered nickel, because its low cost.

The low solubility of hydrogen in the oil, the great size of reactant molecules in the liquid phase, and the high activity of nickel catalysts in these processes, produce that under industrial operating conditions the rate of the reaction is diffusion-controlled. This work presents experimental studies on the hydrogenation of sunflower oil, especially on the *trans*-isomer production. The reaction was performed in a semi-batch reactor with a commercial Ni catalyst, evaluating the pressure, the amount of catalyst and the type of hydrogen bubbling device. The agitation regimen was also considered. These variables were analyzed in relation with the activity and the *cis*-isomers selectivity and the mass transfer resistances.

2. Experimental procedures

2.1. Catalyst and reactants

A commercial silica supported Ni catalyst was used (Ni–SiO$_2$). The manufacturer provided the catalyst in the pre-reduced form inbeded in a solid fat. The data provided by the manufacturer about this catalyst are detailed in Table 1.

Table 1
Characteristics of the Ni–SiO$_2$ commercial catalyst

Content (% wt)	
Ni	22
Silica	4
Fat	74
Structural properties	
Surface specific area (m^2/g)	188
Pore volume (ml/g)	0.23
Main pore diameter (Å)	20
d_p (m)	3E−05
$\rho_{apparent}$ (kg/m^3)	2000
ρ_{bulk} (kg/m^3)	2600

The sunflower oil to be hydrogenated consists of a mixture of: 5.7% C16:0; 3.9% C18:0; 1.5% C18:1t; 38.8% C18:1c; 46.5% C18:2cc; 2.3% C18:2t; 0.3% C20:0; 0.7% C22:0 and 0.3% C24:0 (where the first number represents the total carbon number of the acyl groups and the second number represents the total number of double bonds).

In all the catalytic tests chromatographic grade hydrogen (AGA) was used.

The iodine value (IV) of an oil or fatty acid is the weight of iodine which it combines with, specified as a percentage of its own weight. IV expresses the degree of unsaturation of an oil as:

$$IV = \frac{\text{grams of iodine absorbed}}{100\,\text{g of oil}} \qquad (1)$$

2.2. Catalytic activity measurements

The hydrogenation tests were carried out in a flat-bottom, 0.064 m diameter, 600 ml Parr reactor, operated in a semi-continue manner. The reactor was connected to a hydrogen source, and maintained at constant pressure. The H_2 consumption was measured during the reaction.

The catalytic tests were performed for 1 h using 500 ml of refined sunflower oil. The reduced catalyst was introduced into the reactor containing the sunflower oil at reaction temperature. Then, the pressure was increased in order to start the reaction. The H_2 flow rate versus time curve was corrected by subtracting a similar H_2 flow curve for identical experimental conditions without the catalyst.

The process variables studied and their levels were:

- Reaction temperature: 150, 180, 220 (°C).
- Hydrogen pressure: 207, 414, 620 (kPa).
- Amount of catalyst: 500, 1000, 1500 (mg).
- Agitation rate: 500–1800 (rpm).
- Hydrogen bubbling device: (1) copper tube of 3.2 mm internal diameter, that ends in a ring with 8 holes of 1.6 mm, (2) stainless steel tube of 3.2 mm internal diameter, and (3) stainless steel tube of 1.6 mm internal diameter.
- Stirrer design: a stirrer of inclined blade, a stirrer of 6 vertical blades, and a R100 disc1 (developed by Moucha, Linek, & Prokopova, 2003).

An AGILENT 4890D gas chromatograph (GC) equipped with a flame ionization detector (FID) was used to study the reaction products, following the procedures established by the AOCS Ce 1c-89 norm. A 60-m long SUPELCO 2380 capillary column with a nominal diameter of 0.25 mm and a nominal film thickness of 0.20 μm was used for the separation of the different compounds present in the samples. The iodine number (IV) was calculated from the fatty acid composition following the AOCS Cd 1c-85 norm.

2.3. Solid fat content

Solid fat content (SFC) was calculated in the range between 10 and 50 °C, using a NMR Minispec pc 120 (Bruker) following the procedures established by the AOCS Cd 16b-93 norm.

3. Results and discussion

3.1. Evaluation of diffusional controls

The hydrogenation of sunflower oils over a nickel catalyst is a three-phase system. Fig. 1 shows the profile of hydrogen concentration during the reaction. Two reactants diffusion processes are occurring in a heterogeneous reaction: mass transfer from the bulk to the external surface of the catalyst, and the reactants diffusion from the external surface into the pores of the catalyst.

3.1.1. Diffusion in the gas-phase
The diffusion of hydrogen in the gas bubble has not been considered since the diffusivity in gases is much greater than in liquids. The tests were made with pure hydrogen constantly bubbling in the oil, and the vapor pressure of the oil is negligible at the temperatures of reaction.

3.1.2. Mass transfer in the gas–liquid interphase
Some authors (González-Marcos, Gutiérrez-Ortiz, González-Ortiz de Elguea, Alvarez, & González-Velasco, 1998; Susu, 1982; Veldsink, Bouma, Schöön, & Beenackers, 1997) propose to estimate the magnitude of the different mechanisms for mass transport by plotting the reciprocal of the hydrogenation rate versus the inverse of the catalyst mass according to the following equation:

$$\frac{C_{H_2}}{r_{H_2}} = \frac{1}{k_l a_l} + \frac{1}{m}\left(\frac{1}{k_s a_s} + \frac{1}{k\eta}\right) \qquad (2)$$
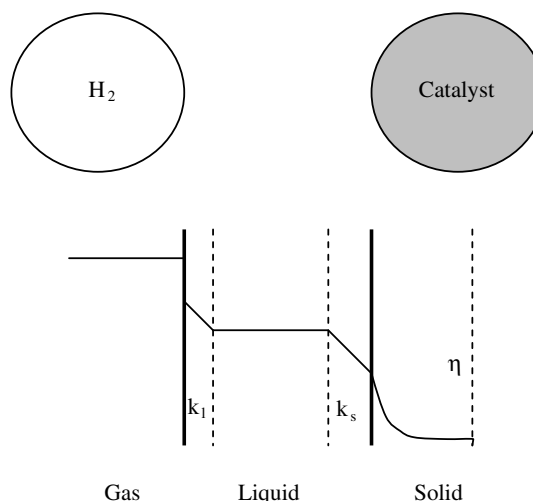

Fig. 1. Profile of hydrogen concentration in a hydrogenation process with agitation.

where C_{H_2} is the H_2 concentration in the liquid–gas interphase, r_{H_2} is the initial reaction rate, k_1 is the coefficient of transfer between the bubble and the liquid, k_s is the coefficient of transfer in the boundary layer that surrounds the catalyst, k is the reaction constant, a_1 and a_s are the areas of transfer between the gas and the liquid, and between the liquid and the solid respectively, η is the effectiveness factor and m the mass of the catalyst. In agreement with this equation, the intercept at the y-axis is associated with the magnitude of the mass transfer resistance between the gas and the liquid, whereas the slope depends on the mass transport processes associated with the catalytic solid.

The standard plot of C_{H_2}/r_{H_2} versus $1/m$ is a straight line only when the reaction order is 1 with respect to the hydrogen concentration (Santacesaria, Parrella, Di Serio, & Borrelli, 1994; Stenberg & Schöon, 1985).

The graph C_{H_2}/r_{H_2} versus $1/m$ for experiments at 700 rpm and 1416 rpm is shown in Fig. 2. In order to make possible a comparison of hydrogenation at different catalyst load, at the same degree of conversion and at the same time of reaction, it is necessary to compare the reaction rates at the start of reaction (Stenberg & Schöon, 1985). The rate of reaction at $t = 0$ was calculated by extrapolation.

In Fig. 2a similar tendency is seen between 700 rpm and 1416 rpm. The curves are characteristic of a system with an order smaller than 1, according to the shape of C_{H_2}/r_{H_2} versus $1/m$ for different reaction orders (Santacesaria et al., 1994).

The volumetric coefficient (k_1a_1) was measured using a 3.0% excess of catalyst (Jonker, 1999). Stenberg and Schöon (1985) demonstrated that the data at high catalyst loading are more accurate because impurities present in natural oils have more pronounced effect on the observed reaction rate at low catalysts loading. k_1a_1 was 0.03 s^{-1} for the reaction at 700 rpm, whereas at 1416 rpm it was 0.1 s^{-1}. This shows that the higher the agitation rate, the higher the volumetric gas–liquid mass transfer coefficient reached.

These values are smaller than the one obtained by Jonker (1999) for a reactor with baffles ($k_1a_1 = 1.8$ s^{-1}).
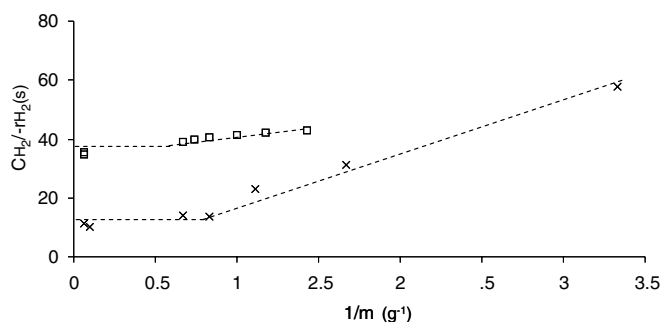

Fig. 2. Representation of Eq. (2) for different agitation regimes. References: □, 700 rpm; x, 1416 rpm. Reaction temperature: 180 °C.

3.1.3. Hydrogen diffusion in the liquid phase

The resistance to the diffusion of hydrogen molecules in the oil can be neglected taking into account that mixing is important due to the agitation and to bubbling of the gas.

3.1.4. Transport in the liquid–solid film

In order to favor the mass transport in the liquid–solid interphase, the relative velocity of the catalyst particle with respect to the liquid must be the highest possible. Nevertheless, in liquid phase processes, the catalyst particle is quite small and tends to move with the liquid. Therefore, the increase of the agitation rate only causes the mixture to go faster, without increasing the relative rate between the liquid and the particle. Due to this, the coefficient of hydrogen mass transfer in the liquid–solid film was estimated using the correlation of Brian and Hales (1969) for spherical particles as proposed by Gutiérrez-Ortiz, Castaño, González-Marcos, Gutiérrez-Ortiz, and González-Velasco (1994)

$$\left(\frac{k_s d_p}{D_i}\right)^2 = 16 + 4.84 \left(\frac{g d_p^3 (\rho_{CAT} - \rho_l)}{18 \mu D_i}\right)^{2/3} \quad (3)$$

where D_i is the diffusivity of reactant in the liquid phase, ρ_l is the liquid density and ρ_{CAT} is the apparent density of the catalyst particle. The viscosity of liquid phase is μ, d_p is the mean particle diameter and g is the acceleration due to gravity. The liquid–solid mass transfer coefficient k_s was 9.7×10^{-4} m s^{-1} (at 100 °C). Santacesaria et al. (1994) reported a value of 1.2×10^{-3} m s^{-1} for k_s (at 100 °C) using the semiempirical relation suggested by Sano, Yamaguchi, and Adachi (1974).

3.1.5. Intraparticle mass transfer

There are intraparticle concentration gradients caused by limitations in the reactant and products mass transfer within the catalyst.

The effectiveness factor η is a measure of the effective usage of the catalyst particle space, which is a function of the Thiele modulus (ϕ). The effectiveness factor is a function of temperature, pressure and catalyst properties such as shape, size and diffusivity of components.

$$\eta = \frac{\text{observed reaction rate}}{\text{max. rate if all surface exposed to } C_{iS}} = \frac{-r_{obs,i}}{r_{i_S}} \quad (4)$$

where C_{iS} is the surface concentration. The Thiele modulus for a spherical particle and a first order reaction, is:

$$\phi^2 = \frac{\text{reaction rate at } C_{iS}}{\text{diffusion rate}} = \frac{-r_{i_S} \rho_p R_p^2}{D_{eff\,i} C_{iS}} \quad (5)$$

where D_{eff} is the effective diffusion (m^2/s m$^3_{liq}$/m$^3_{cat}$), R_p indicates the main particle radius (m), ρ_p is the apparent density of the catalyst (g/cm^3) and r_{obs} is the initial observed rate of consumption (mol/s kg$_{cat}$). C_{iS} can be considered the concentration of sunflower oil or H_2 (mol/m^3). The rate of reaction at $t = 0$ can be calculated by extrapolation.

Φ		Operation conditions			
H_2	Triglycerides	T (°C)	P (kPa)	Catalyst load (g)	D^a
59.6	9.0	180	207	0.5	1
27.1	8.2	180	414	1.0	2
16.8	7.7	180	620	1.5	3
49.7	5.7	200	207	1.0	3
32.9	7.6	200	414	1.5	1
87.9	30.5	200	620	0.5	2
8.7	1.9	160	207	1.5	2
15.1	6.8	160	414	0.5	3
15.6	10.5	160	620	1.0	1

[a] D = bubbling devices.

The following equation is an expression of the functionality between η and ϕ (*again, first order reaction*)

$$\eta = \frac{\tanh(\phi)}{\phi} \qquad (6)$$

For η near unity, the entire volume of the catalyst particle is reacting at the same high rate because the reactant is able to diffuse quickly through the particle. For η near zero, the particle reacts at a low rate. The reactant is unable to penetrate significantly into the interior of the particle and the reaction rate is small in a large portion of the particle volume.

For large values of the Thiele modulus, the rate of reaction is much greater than the rate of diffusion, the effectiveness factor is much less than unity, and the reaction is diffusion limited. Conversely, when the diffusion rate is much larger than the reaction rate, the effectiveness factor is near unity.

If the reaction rate expression is not known beforehand, the Weisz–Prater module (Φ) can be used in order to estimate the intraparticle gradients.

$$\Phi i = \frac{\text{observed reaction rate}}{\text{diffusion rate}} = \eta.\phi^2 = \frac{(-r_{\text{obs},i})\rho_p R_p^2}{D_{\text{eff},i} C_{iS}} \qquad (7)$$

For $\Phi \ll 1$, it is possible to consider that there is no intraparticle mass transfer. On the other hand, when $\Phi \gg 1$ severe diffusion limitation are presents.

The calculated Φ values from the reaction rates measured for different operation conditions are shown in Table 2. Tables 1 and 3 detailed the data used for the calculation.

Considering the ϕ values obtained, it is not possible to neglect the concentration gradients within the catalyst particle.

The *trans*-isomers formation depends heavily on the Weisz–Prater module (Fig. 3). The reason being the effect of the hydrogen availability on the surface catalyst. When there are not limitations for the hydrogen molecule to reach at the metal, an excess of gas will exist on the active site, and the triglyceride molecule will tend to saturate before the isomerization.

However, when the restrictions on the hydrogen are significant (at high values of Weisz–Prater module), a lower amount of saturated compound will be produced as it can be observed in Fig. 4. In this figure the ϕ value for C18:0 at IV = 110 has been omitted, since there was no
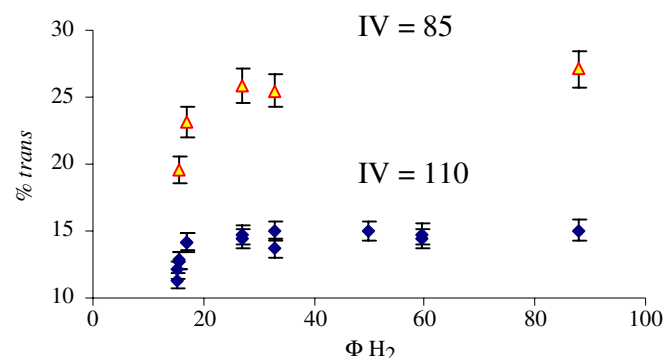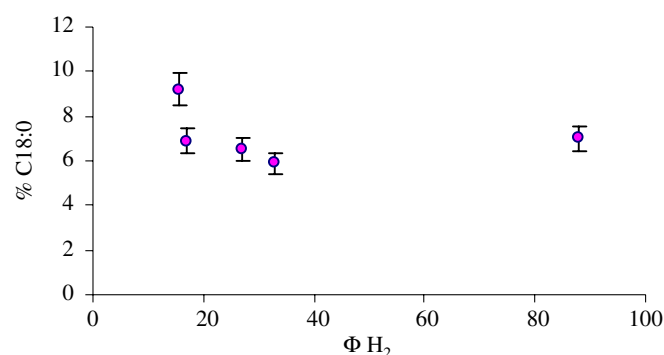

Fig. 3. *Trans*-isomers formation versus Weisz–Prater module.

Fig. 4. C18:0% versus Weisz–Prater module (IV = 85).

Table 3
Data for the determination of the Weisz–Prater module

	T (°C)			Source
	160	180	200	
ρ_{oil} (kg/m³)	826	815	801	Allen et al. (1982)
$D_{\text{H2,eff}}$ (m²/s)	1.20E−10	1.48E−10	1.98E−10	Andersson et al. (1974)
$D_{\text{Tg,eff}}$ (m²/s)	2.9E−12	3.5E−12	4.0E−12	Jonker (1999)
C_{Tg} (kmol/m³)	0.093	0.091	0.094	

Porosity: $\varepsilon = 0.24$; tortuosity: $\tau = 34$ Jonker (1999).

increase of the saturated component due to the low extent of reaction.

3.2. Reaction order

Reaction orders between 0 and 1 for the hydrogen concentration have been reported by Susu (1982) and Jonker (1999). For the concentration of oil species a Langmuir–Hinshelwood adsorption mechanism is assumed, which is of pseudo first order (Gut, Kosinka, Prabucki, & Schuerch, 1979). Jonker (1999) finds a good correlation of his data with a Langmuir–Hinshelwood–Hougen–Watson adsorption model for the monounsaturated fatty acid methyl ester.

To test the rate equations properly, we performed a new type of tests. In these experiments, the autoclave was operated in a batch manner. Hydrogen was consumed from the head space of the autoclave without additional supply from the storage bottle. Fig. 5 shows the variation of the hydrogen pressure with the reaction time (operation conditions: 160 °C and 700 rpm).
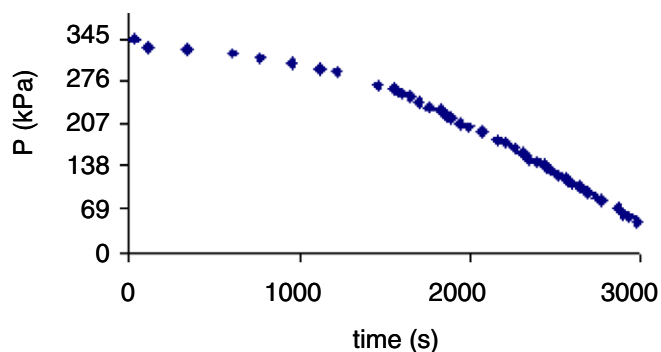

Fig. 5. Reactor pressure during a typical experiment with varying hydrogen pressure. Conditions: 160 °C, 0.26 kg cat/m³ oil, 700 rpm.
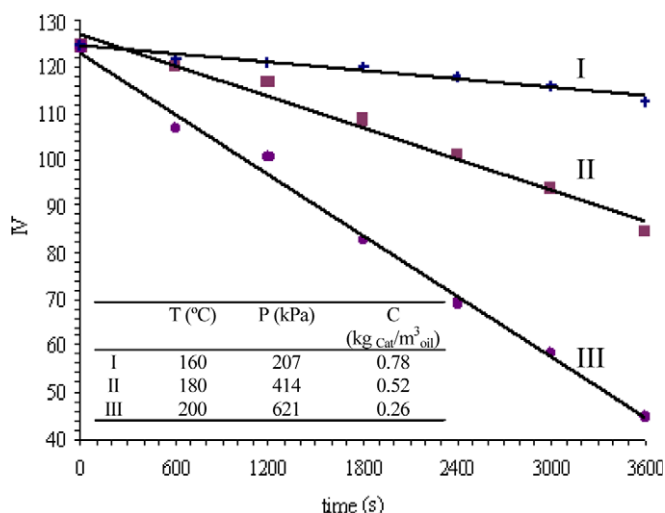

Fig. 6. IV versus reaction time in a semibatch reactor (700 rpm).

After an initial transient time, where the pressure varies slightly, a linear dependency of pressure on time is seen, it could indicate a reaction order of 0 with respect to hydrogen during this period of reaction.

Fig. 6 shows the decrease of the IV of the sunflower oil, during the hydrogenation process carried out in a semibatch reactor. In all the reactions performed at 700 rpm, the graph presents a good linear correlation between IV and the reaction time. This is corroborated by the graph $C_{H_2}/-r_{H_2}$ versus $1/m$ (Fig. 2).

3.3. Variables of the process

3.3.1. Stirrer design

A high mixed efficiency of the stirrers leads to an improvement in the mass transfer in a three-phase system. It also originates a good dispersion of the catalyst and the gas in the reactor.

Three different stirrers design were used: (a) a stirrer of inclined blade, similar to the A200 stirrer of axial flow shown by Patterson (1994), (b) a stirrer of six vertical blades, and (c) a R100 disc, developed by Moucha et al. (2003).

Fig. 7 presents the advance of the reaction versus the reaction time. The graph shows the greater efficiency of the stirrer with inclined blade (axial flow), with respect to that of vertical blades (radial flow). The reaction was carried out at 180 °C and 620 kPa, with 0.26 kg$_{cat}$/m³$_{oil}$ and using a bubbling device consisting of a Cu ring with perforations for the hydrogen supply.

Rieger, Ditl, and Novák (1979) made a study to determine the depth of the vortex in stirred baffleless tanks with vertical flat blades and inclined blades (different number of blades). They used different Newtonian fluids, finding an equation based on the Froude number (Fr), the Galileo number (Ga) and the relation of the stirrer and the reactor diameters (d_s/d_r). For low Galileo numbers they found the following expression to calculate the depth of the vortex (h_l):

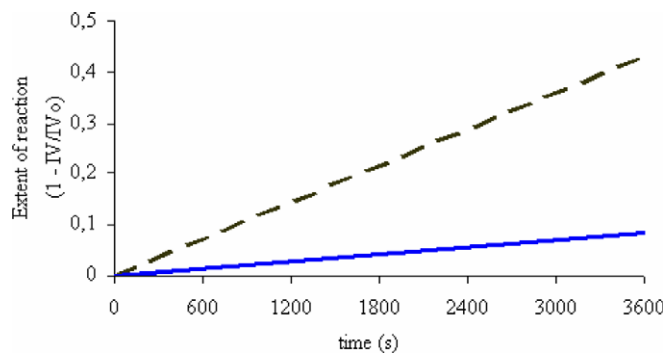

Fig. 7. Extent of reaction versus reaction time for different stirrers. Operation conditions: 700 rpm, 180 °C, 620 kPa, with 0.26 kg cat/m³ oil. References: (- - -) stirrer with inclined blade, (—) stirrer with vertical blades.

$$\frac{h_1}{d_s} = B_1 Ga^{0.33} \left(\frac{d_r}{d_s}\right)^{-1.18} Fr^{\left[3.38 Ga^{-0.074} \left(\frac{d_r}{d_s}\right)^{0.14}\right]} \qquad (8)$$

The calculated vortex depths were 0.04 m and 0.07 m for the stirrer of inclined blade and of vertical blades respectively. The values of the parameters used in Eq. (8) are shown in Table 4.

From the data it can be inferred that the vortex was deeper for the stirrer with radial flow (vertical blades), demonstrating a minor mixing. Under these conditions, the gas dispersion in the liquid was low, influencing the rate of reaction in an unfavorable way.

Both Reynolds numbers, laboratory and full-scale reactors, are larger than 10^4. Thus, the flow in the stirred tank is fully turbulent. Under this condition, the impeller outflow profiles are typically independent of Reynolds number.

3.3.2. H_2 bubbling device

Different tests were made with three types of hydrogen bubbling devices. The three models were: (1) copper tube of 3.2 mm internal diameter, that ends in a ring with 8 holes of 1.6 mm, (2) stainless steel tube of 3.2 mm internal diameter, and (3) stainless steel tube of 1.6 mm internal diameter.

The hydrogenation was performed at 180 °C and 620 kPa, during 1 h with 0.26 kg_{cat}/m^3_{oil} and 700 rpm (Fig. 8). The averages of the three analyzed populations ($D = 1$, 2 and 3) were not significantly different from a level of confidence $\alpha = 5\%$ (ANOVA).

In the reaction experiments hydrogen is supplied to the reactor at a rate of 549 cm^3/min in the opening of the bubbling device. At this regime, the orifice diameter and the gas-in-orifice speed have a weak influence on the diameter of the bubble. This diameter depends mainly on the turbulence in the continuous phase (Sideman, Hortacsu, & Fulton, 1966), which probably generates a similar dispersion of bubbles in models 2 and 3.

No significant differences were observed in the copper ring in the extent of reaction. This can be attributed to a strong influence of the generated shear stress between thin layers of liquid that quickly one over the other, as opposed to the influence of the amount of generated bubbles. These
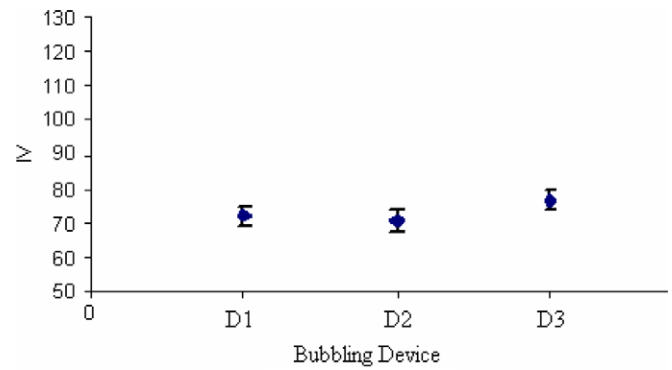

Fig. 8. IV for different bubbling devices. References, D1: copper tube of 3.2 mm internal diameter, that ends in a ring with 8 holes of 1.6 mm; D2: stainless stele tube of 3.2 mm internal diameter; D3: stainless stele tube of 1.6 mm internal diameter.

efforts, caused by the agitation, generate the rupture of the gas bubbles and facilitate their physical solution.

3.3.3. Effect of the agitation rate

Some authors confirm the lack of resistance to mass transfer in the gas–liquid interphase when the hydrogenation rate is independent of the agitation rate (Susu, 1982; Wisniak & Stein, 1974). Nevertheless, a high agitation rate not always is equivalent to a liquid phase intensely mixed due to the possible formation of vortices. Thus, additional determinations should be carried out (Veldsink et al., 1997), like those shown in Section 3.1.

Fig. 9 shows the activity variation versus the agitation rate. It can be observed that over 1000 rpm the activity is invariant. The zone below 1000 rpm indicates that as the agitation regime rises it increases hydrogen concentration, favoring the hydrogenation reaction.

For the present case, it is not possible to avoid the presence of mass intraparticle resistance working at high agitation rate. Even though $k_s \to \infty$, the effectiveness factor, η, must necessarily be low given the characteristics of the catalyst.

3.3.4. Temperature

Temperature favors the hydrogenation and isomerization reactions, increasing the demand of hydrogen in the

Table 4
Values used for the calculation of the vortex depth

	Stirrer with inclined blade	Stirrer with vertical blades	Source
d_r (m)	0.064	0.064	
d_s (m)	0.035	0.035	
N (rev/s)	11.8	11.8	
ρ_{oil} (kg/m³)	815	815	Allen et al. (1982)
μ_{oil} (kg/(m s))	0.005	0.005	Allen et al. (1982)
g (m/s²)	9.8	9.8	
Re[a]	2355[a]	2260[a]	
Fr	0.5	0.5	
Ga	1.1E+07	1.0E+07	
B[b]	0.020[b]	0.046	Rieger et al. (1979)

[a] Re on full-scale reactor = 2×10^6.
[b] Average value between the values used by Rieger et al. (1979) for 3 and 6 inclined blades (0.013 and 0.029 respectively).
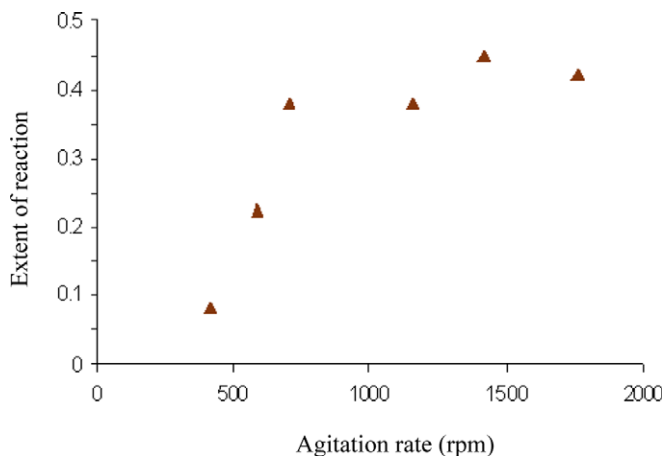
Fig. 9. Activity versus agitation rate. Reaction time: 30 min. Operation conditions: $0.26\ kg_{cat}/m^3_{oil}$, 414 kPa.

catalyst surface. The effect of the temperature on *cis* and *trans*-isomers can be observed in Fig. 10.

Studying *trans*-isomers production at 150 °C, 180 °C and 220 °C with the Analysis of Variance (ANOVA) technique, it is possible to conclude that these tests were significantly different with a confidence level of 5%.

The production of *cis*-isomers in samples extracted at different times during the hydrogenation test performed at three different temperatures (with $IV_{end/final} = 108$ in all the cases) was not significantly different (ANOVA, confidence level = 5%).

The increase of the reaction temperature promotes the *trans*-isomerization, without affecting the total *cis*-isomer content, which allows inferring that temperature is a variable with a significant influence on the control of *trans*-isomer production at 700 and 1416 rpm (the 700 rpm-test is not shown here).

The reaction rate in the catalytic experiments at different temperatures was noticeably different. When the hydroge-

nation was carried out at 150 °C, a IV = 108 was obtained in a reaction time of 140 min, while at 220 °C the reaction reached the same IV in only 5 min.

3.4. Selectivity

3.4.1. Oleic/linoleic selectivity

The distribution of reaction products (Fig. 11) follows the typical tendency of a consecutive reaction:

$$C18:2 + H_2 \xrightarrow{k_2} C18:1 + H_2 \xrightarrow{k_1} C18:0 \qquad (9)$$
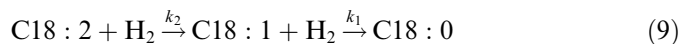
where C18:2, C18:1 and C18:0 are the concentrations of linoleic, oleic and stearic acids, and k_1 and k_2 are the corresponding rate constants.

Vegetable oil hydrogenation includes a series of collateral reactions (as geometrical and position isomerization). However, as a first approximation to the evaluation of the catalyst selectivity, Eq. (9) is a good representation of the reaction mechanism. The hydrogenation of linolenic acid (C18:3) is not considered, due to its low initial concentration in sunflower oil (less than 0.4%).

Fig. 12 shows the C18:1 to the initial C18:2 concentrations ratio (relates to oleic selectivity) as a function of the linoleic concentration (indicates the extent of the double bond conversion). In this figure, the data collected during tests performed at 700 and 1416 rpm are differentiated. It is observed that practically all the experimental information seems to respond to the same functionality for a specific agitation regime. A plot of this sort is obtained as the solution for a set of differential equations describing the time-dependent behavior of a series reacting system like Eq. (9). The solution of that set of equations is:
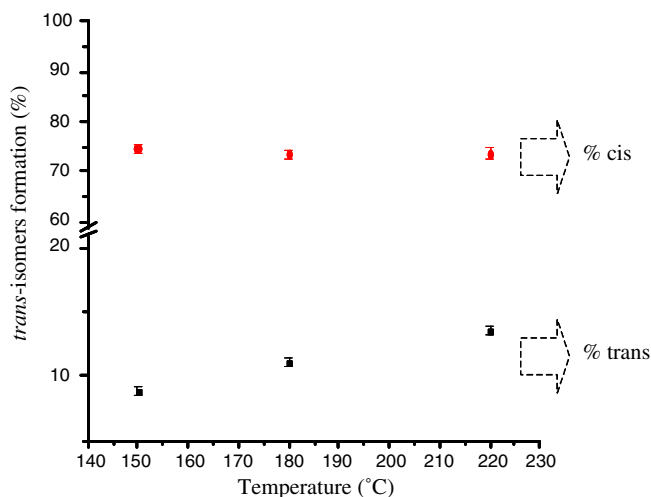

Fig. 10. *trans*-Isomers formation versus reaction temperature (IV = 108). Operation conditions: $0.26\ kg_{cat}/m^3_{oil}$, 1416 rpm and 414 kPa.
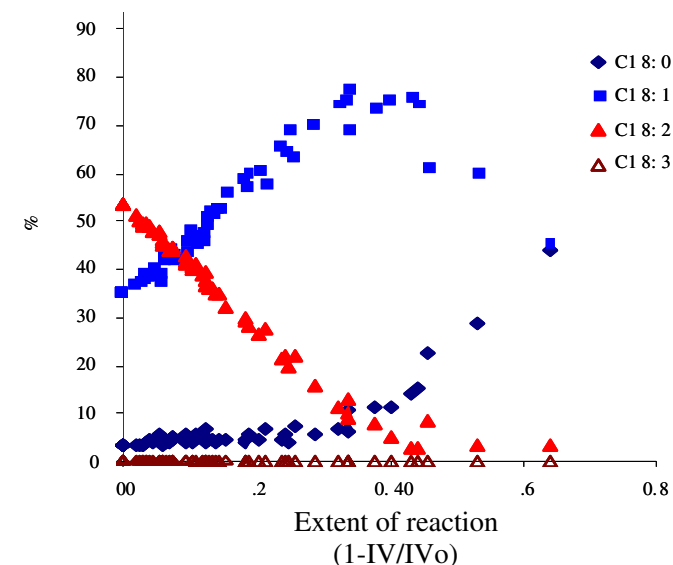

Fig. 11. Reaction product distribution versus the extent of reaction. Agitation rate: 700 rpm.
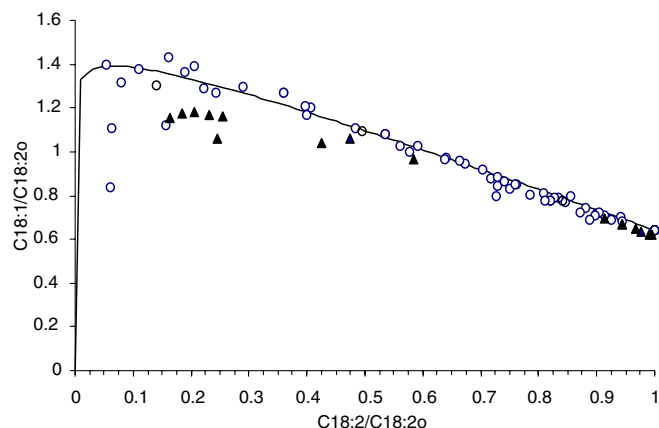
Fig. 12. Selectivity towards oleic acid (C18:1) as a function of C18:2 conversion. Reference: ○ 700 rpm, ▲ 1416 rpm (solution for $\alpha = 0.046$ and $\beta = 0.965$).

Fig. 13. Solid fat content profiles of partially hydrogenated sunflower oil (NMR).

$$\frac{C18:1}{C18:2_0} = \frac{\beta}{1-\alpha}\left[\left(\frac{C18:2}{C18:2_0}\right)^{\alpha} - \left(\frac{C18:2}{C18:2_0}\right)\right]$$
$$+ \left(\frac{C18:2}{C18:2_0}\right)^{\alpha}\left(\frac{C18:1_0}{C18:2_0}\right) \qquad (10)$$

where α and β depend on the kinetic constants, the transport coefficients and the hydrogen concentration.

The data appear grouped following two different solutions of the set of equations. Specially at low $C18:2/C18:2_0$ values the set of data containing experimental results obtained at a different agitation regime differ appreciably. This can be due to the effect of the higher agitation regime on the external mass transfer resistance. However, within each group, the selectivity is not considerably influenced by operative variables like temperature, pressure or catalyst mass. This could indicate that the linoleic/oleic selectivity will be determined by the extent of reaction in the presence of intraparticle diffusional controls when temperature and hydrogen pressure are moderately changed.

3.5. Solid fat content

Fig. 13 displays the curves of solid fat content (SFC) as a function of the temperature. SFC refers to the amount of solid present in the oil. The hardening process is critical for small changes of the IV, and has substantial effects on the SFC. Oils with greater degree of hydrogenation melt at higher temperatures. The SFC not only increases with the saturation of the double bonds, but also with the amount of *trans*-isomers.

It is important to emphasize the different behavior of curves "b" and "c" in spite of having the same IV. This is explained by a difference in the saturated content (similar IV for different original oleic–linoleic ratio). The sample with a greater amount of saturated compounds contains a higher amount of solids (because these are solid in the temperature range analyzed, unlike the mono and polyunsaturated compounds with *cis* chains). Samples "a" and "b" present a high SFC at 25 °C, indicating that at room
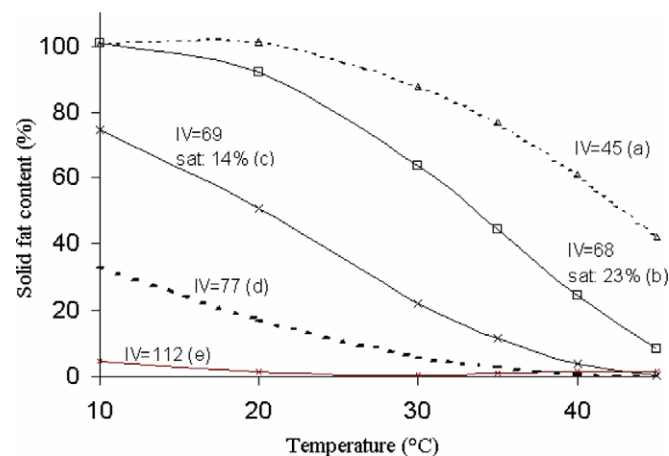
temperature they are hard and fragile fats. The fat represented by curve "a" has elevated SFC value at body temperature (37 °C), that gives a waxy sensation in the mouth (Dubinsky, 1995).

The fundamental difference between the two samples presented in Fig. 14 is the relation between *trans*-isomers and saturated compounds (Table 5). There is a distinction between the oleic and linoleic amount, but this would not affect the solid content, since both behave in similar ways in the analyzed temperature range. A difference in the melting range can be seen: the smaller *trans*-isomers amount and the greater saturated compound amount in sample "d" (hydrogenation performed at 620 and 414 kPa) generates a curve of lower slope with respect to sample "f" (reaction carried out at 200 °C and 620 kPa), which indicates a greater melting range. Both samples had a greasy consistency at room temperature, and solid at refrigerator temperature (8 °C).

As the reduction of the curve becomes steeper the fat becomes relatively liquid as the temperature rises slightly. If this happens at few degrees below the body temperature, the fast melting of the fat has as result a refreshing sensation in the palate (Dubinsky, 1995). The SFC curve required will be determined by the application of the final product.
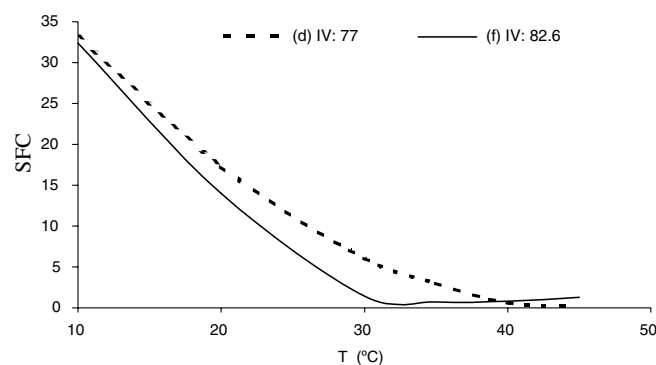

Fig. 14. Comparison of SFC curves.

Table 5
Fatty acid distribution for curves (d) and (f) of Fig. 14

Component	(d)	(f)
C16.0	6.2	6.2
C18.0	7.2	11.3
C18.1t	25.5	20.3
C18.1c	49.6	53.2
C18.2t	2.6	2.9
C18.2c	7.8	5.0
C18.3	0.0	0.0
C20.0	0.3	0.3
C22.0	0.7	0.7

4. Conclusions

When the experiments were conducted in diffusional regime, activity and selectivity appear to be independent of the hydrogen bubbling system and the catalyst loading.

The presence of diffusional controls strongly reduces the possibility of altering the oleic/linoleic selectivity of the catalyst. Thus, the *cis–trans* selectivity is function only of the extent of reaction.

The intraparticle diffusional control (evaluated by the Weisz–Prater module) has a great influence on the *trans*-isomer formation, because the diffusional limitations cause a hydrogen deficiency in the catalytic surface. This is the limiting factor of the reaction rate and is critical for the isomerization reactions.

Acknowledgements

References

Allen, R., Formo, M., Krishnamurthy, R., McDermott, G., Norris, F., & Sonntag, N. (1982) (4th ed.). In D. Swern (Ed.). *Bailey's industrial oil and fat products* (Vol. 2). Wiley.

Andersson, K., Hell, M., Löwendahl, L., & Schöön, N. H. (1974). Diffusivities of hydrogen and gliceryl trioleate in cottonseed oil at elevated temperature. *Journal of the American Oil Chemists' Society, 51*(4), 171–173.

Ascherio, A., Katan, M., Zock, P., Stampfer, M., & Willett, W. (1999). Trans fatty acids and coronary heart disease. *The New England Journal of Medicine, 340*, 1994–1998.

Brian, P. L. T., & Hales, H. B. (1969). Effects of transpiration and changing diameter on heat and mass transfer to spheres. *AIChE Journal, 15*, 419–435.

Dijkstra, A. J. (1997). Hydrogenation revisited. *Inform, 8*, 1150–1158.

Dubinsky, E. (1995). Productos hidrogenados: producción y especificaciones. *Aceites y Grasas, 19*, 192–203.

González-Marcos, M. P., Gutiérrez-Ortiz, J. I., González-Ortiz de Elguea, C., Alvarez, J. I., & González-Velasco, J. R. (1998). Control of the product distribution in the hydrogenation of vegetable oils over nickel on silica catalysts. *Canadian Journal of Chemical Engineering, 76*(5), 927–935.

Gut, G., Kosinka, J., Prabucki, A., & Schuerch (1979). A kinetics of the liquid-phase hydrogenation and isomerization of sunflower seed oil with nickel catalysts. *Chemical Engineering Science, 34*, 1051–1056.

Gutiérrez-Ortiz, M. A., Castaño, A., González-Marcos, M. P., Gutiérrez-Ortiz, J. I., & González-Velasco, J. R. (1994). Influence of operational variables on the catalytic behavior of Pt/alumina in the slurry-phase hydrogenation of phenol. *Industrial & Engineering Chemistry Research, 33*(11), 2571–2577.

Jonker, G. H. (1999). *Hydrogenation of edible oils and fats*, PhD thesis. The Netherlands: Groningen University.

Mensink, R., & Katan, M. (1990). Effect of dietary trans fatty acids on high-density and low-density lipoprotein cholesterol levels in healthy subjects. *The New England Journal of Medicine, 323*, 439–445.

Mondal, K., & Lalvani, S. (2000). Second order kinetics of catalytic transfer hydrogenation. *Journal of the American Oil Chemists' Society, 77*, 1–8.

Moucha, T., Linek, V., & Prokopova, E. (2003). Gas hold-up, mixing time and gas–liquid volumetric mass transfer coefficient of various multiple-impeller configurations: Rushton turbine, pitched blade and techmix impeller and their combinations. *Chemical Engineering Science, 58*(8), 1839–1846.

Patterson, H. B. W. (1994). *Hydrogenation of fats and oils: theory and practice*. Champaign: American Oil Chemists' Society, pp. 56–58.

Rieger, F., Ditl, P., & Novák, V. (1979). Vortex depth in mixed unbaffled vessels. *Chemical Engineering Science, 34*, 397–401.

Rodrigo, M. T., Daza, L., & Mendioroz, S. (1992). Nickel supported on natural silicates. Activity and selectivity in sunflower seed oil hydrogenation. *Applied Catalysis A: General, 88*(1), 101–114.

Sano, Y., Yamaguchi, N., & Adachi, T. (1974). Mass transfer coefficients for suspended particles in agitated vessels and bubble columns. *Journal of Chemical Engineering of Japan, 7*, 255–261.

Santacesaria, E., Parrella, P., Di Serio, M., & Borrelli, G. (1994). Role of mass transfer and kinetics in the hydrogenation of rapeseed oil on a supported palladium catalyst. *Applied Catalysis A: General, 116*(1–2), 269–294.

Sideman, S., Hortacsu, O., & Fulton, J. W. (1966). Mass transfer in gas–liquid contacting systems. *Industrial & Engineering Chemistry, 58*(1), 32–47.

Stenberg, O., & Schöön, N.-H. (1985). Aspects of the graphical determination of the volumetric mass-transfer coefficient ($k_L a$) in liquid-phase hydrogenation in a slurry reactor. *Chemical Engineering Science, 40*(12), 2311–2319.

Susu, A. (1982). Mass transfer and scale-up in Ni catalyzed oil hydrogenators. *Applied Catalysis, 4*(4), 307–320.

Veldsink, J. W., Bouma, M. J., Schöön, N. H., & Beenackers, A. A. C. M. (1997). Heterogeneous hydrogenation of vegetable oils: a literature review. *Catalysis Reviews, 39*(3), 253–318.

Wisniak, J., & Stein, S. (1974). Hydrogen solubility in jojoba oil. *Journal of the American Oil Chemists' Society, 51*, 482–485.